Hydrometallurgy 169 (2017) 59–67

Contents lists available at ScienceDirect

Hydrometallurgy

journal homepage: www.elsevier.com/locate/hydromet

Selectivity potential of ionic liquids for metal extraction from slags containing rare earth elements

Ayfer Kilicarslan Sahin [a,b,*], Daniel Voßenkaul [a], Nicolas Stoltz [c], Srecko Stopic [a], Muhlis Nezihi Saridede [b], Bernd Friedrich [a]

[a] RWTH Aachen University, IME Department of Process, Metallurgy and Metal Recycling, Intzestraße 3, 52072 Aachen, Germany
[b] Yildiz Technical University, Department of Metallurgy and Materials Engineering, Davutpasa Campus, Esenler, 34210 Istanbul, Turkey
[c] RWTH Aachen University, IML Institute of Mineralogy and Economic Geology, Wüllnerstraße 2, 52072 Aachen, Germany

ARTICLE INFO

Article history:
Received 25 March 2016
Received in revised form 8 December 2016
Accepted 8 December 2016
Available online 11 December 2016

Keywords:
NiMH battery
Rare earth
Ionic liquid
Recovery
Hydrometallurgy
QEMSCAN

ABSTRACT

The recycling of rare earth elements and base metals from recycling slag powders of nickel metal hydride (NiMH) batteries by ionic liquid leaching was studied. Leaching tests were conducted by using the ionic liquid 1-methylimidazolium hydrogen sulfate ($HmimHSO_4$) selected after some preliminary leaching tests on slag powders. The $HmimHSO_4$ concentration of aqueous ionic liquid solution was 30% (v/v) in all tests. The slag powders were ground and sieved to obtain two different particle-size fractions namely 63–90 μm and 90–125 μm in order to evaluate the leaching behavior and the kinetics. The most important metals present in the initial slag powders are iron (35.70% w/w), aluminum (9.95% w/w), manganese (3.45% w/w) and rare earth elements (REEs) such as lanthanum, cerium, neodymium and yttrium (totally 22.50% w/w). In the leaching experiments three parameters were studied: temperature, particle size and time. The average dissolution ratios of 63–90 μm particle size slag powder were 100% for iron, manganese and yttrium after 2 h at a temperature of 80 °C. However, the maximum leaching efficiencies were about 15% for lanthanide and cerium and 20% for neodymium under the same conditions. As an explanation for the low recovery rates, a phase analysis with QEMSCAN (**Q**uantitative **E**valuation of **M**aterials by **SCAN**ning electron microscopy) indicated decomposition in the initial REE phases but a precipitation as sulfates. The kinetic study of Fe and Mn dissolutions showed that the leaching process follows the shrinking core model with an unchanged particle size controlling diffusion through the product layer.

1. Introduction

The rare earth elements (REEs) comprise seventeen elements being the fifteen lanthanide series plus yttrium and scandium which are chemically similar to each other (Jordens et al., 2013; Binnemans et al., 2013). Because of their unique magnetic, luminescent, and electrochemical properties, they are vital to many high-tech industries including consumer electronics, computers, networks, communications, clean energy, advanced transportation, health care, national defense and many others (Massari and Ruberti, 2013; Xie et al., 2014). Since rare earth resources are eccentrically located in some countries, supplying them is affected by political situations or economic affairs (Itoh et al., 2009). In addition to the primary sources, wastes such as spent catalysts, super-alloy scrap, spent batteries, sludge and dusts are potential secondary sources of REEs (Pietrelli et al., 2002). It is necessary to develop efficient recycling processes to recover REEs from secondary sources due to the high prices of the commodities and the environmental impacts of mining.

Spent NiMH batteries are one of the important REE sources, consisting of lanthanum, cerium, praseodymium, neodymium and yttrium together with significant amounts of valuable metals like nickel and cobalt. At the Institute of Process Metallurgy and Metal Recycling (IME) a process was developed to recycle NiMH batteries by Müller and Friedrich at RWTH Aachen University, Germany (Al-Thyabat et al., 2013). In the process, scrap batteries were firstly crushed and sieved to remove iron and plastic, then the crushed battery scrap was melted in an electric arc furnace in order to produce a nickel-cobalt alloy and a slag phase highly enriched with REE-oxides. The produced Ni-Co alloy is already a marketable product for direct use as a battery alloy component. The slag which is highly rich in REEs might be a satisfactory raw material for the production of REEs (Müller and Friedrich, 2006; Al-Thyabat et al., 2013; Weyhe et al., 2002).

Some previous research has proposed hydrometallurgical recycling processes for the NiMH batteries using conventional acid leaching using H_2SO_4 or HCl (Pietrelli et al., 2002; Innocenzi and Vegliò, 2012). However, in these hydrometallurgical processes, the treatment of a large amount of wastewater is required (Innocenzi and Vegliò, 2012).

* Corresponding author at: Yildiz Technical University, Department of Metallurgy and Materials Engineering, Davutpasa Campus, Esenler, 34210 Istanbul, Turkey.
E-mail address: kilicarslanayfer@gmail.com (A.K. Sahin).

http://dx.doi.org/10.1016/j.hydromet.2016.12.002
0304-386X/

Table 1
The chemical composition of NiMH battery slag powder samples (mass fraction).

Element (%)	Fe	Mn	Al	Ni	Ca	K	Na	Si	La	Ce	Nd	Y
Fine fraction (63–90 μm)	35.70	3.45	9.95	0.08	2.33	1.93	0.85	4.43	10.10	8.83	2.48	0.16
Coarse fraction (90–125 μm)	34.60	3.49	10.00	0.12	2.32	2.03	0.93	4.95	10.70	9.30	2.67	0.17

Recently, ionic liquids (ILs) have been studied as novel solvents for the sustainable dissolution, extraction and separation of metal ions (Han and Row, 2010; McCluskey et al., 2002; Kılıçarslan and Sarıdede, 2016). Ionic liquids are organic salts, generally with a low melting point (<100 °C) (Welton, 1999). A remarkable variation is possible in both the anionic and cationic part of the IL and thus it is possible to create an IL with the desired properties to meet the requirements of a particular process (Earle and Seddon, 2000). The ILs have excellent properties including negligible vapor pressure, non-flammability, a wide liquid range and the thermal stability to solubilize a wide range of solutes including metal salts and complexes. Especially, their ability to dissolve a variety of non-ferrous oxides and hydroxides at low temperatures makes the ILs attractive and a green alternative to the traditional aqueous acid/alkaline solutions used in the hydrometallurgical processes which are associated with large volumes of effluent production and require elevated temperatures and pressures (Guo-cai et al., 2010).

So far, ionic liquids have been studied as solvents in different leaching systems for the extraction of transition metals, gold and silver from their concentrates. McCluskey et al. (2002) investigated the use of 1-butyl-3-methyl-imidazolium tetrafluoroborate ([Bmim]BF_4) as the ionic liquid with $Fe(BF_4)_3$ in the leaching process of chalcopyrite and reported that after 8 h with $Fe(BF_4)_3$ in water ([Bmim]BF_4 of 1:1) an extraction of 90% of copper was achieved at 100 °C. Whitehead et al. (2004) studied the leaching of gold and silver from ores in 1-butyl-3-methyl-imidazolium hydrogen sulfate as the ionic liquid ([Bmim]HSO_4) in combination with iron(III) sulfate as oxidant and thiourea. The recoveries of 87% gold and ≥60% silver were achieved with the relatively selective extraction process over the other metals (Cu, Zn, Pb, Fe) which were present in the concentrate. In the same study, successful extraction of gold, silver and base metals (Cu, Zn, Pb, Fe) was also reported using [Cmim][CF_3SO_3] (Whitehead et al., 2007). Dong et al. (2009) investigated the leaching of chalcopyrite using [Bmim]HSO_4 as the ionic liquid and indicated that the copper extraction increased from 51.8% to 87.8% as the ionic liquid concentration in the leaching solution increased from 10% (v/v) to 100%. Beyond that, the leaching behavior of copper from waste printed circuit boards using the same ionic liquid was studied by Huang et al. and they found that the copper leaching ratio was almost 100% in 25 mL of 80% (v/v) of the ionic liquid with a combination of 10 mL of 30% hydrogen peroxide (Aydogan et al., 2006).

In this study, the leaching of NiMH battery slag powders from a process, for the recovery of base and rare metals developed at the IME, was investigated by using ionic liquid 1-methylimidazolium hydrogen sulfate (HmimHSO_4). The kinetics of the leaching process were analyzed

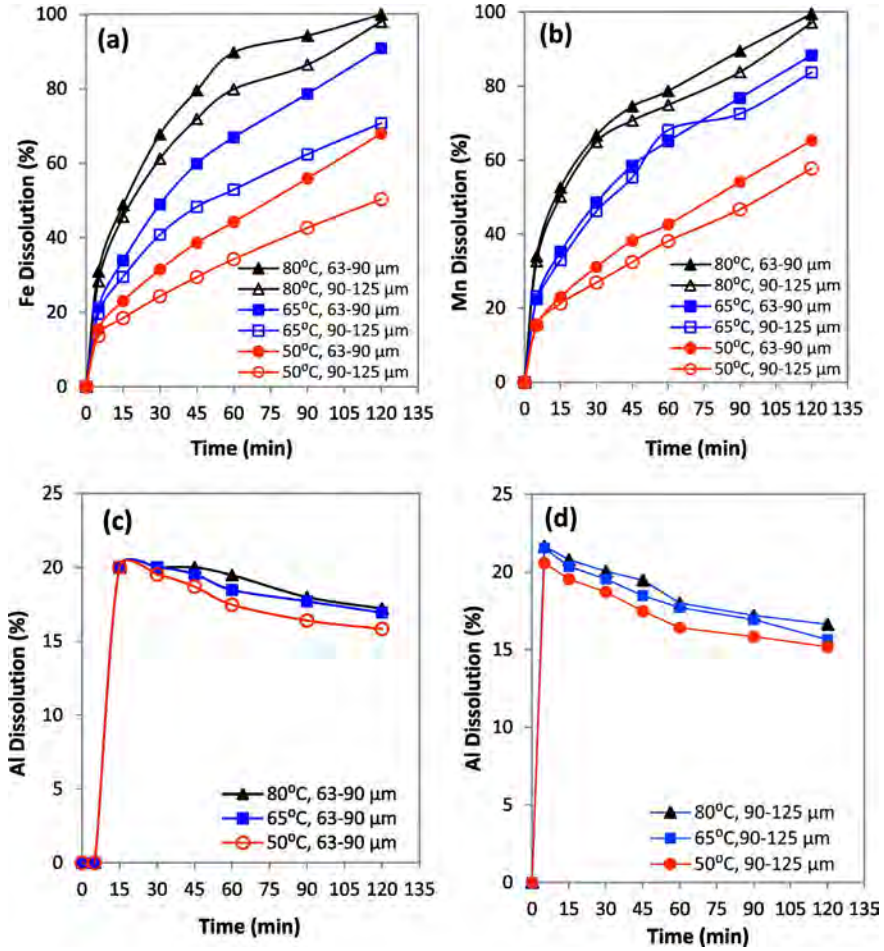

Fig. 1. Effect of particle size on leaching efficiency (a) Fe, (b) Mn, (c) Al (63–90 μm), (d) Al (90–125 μm).

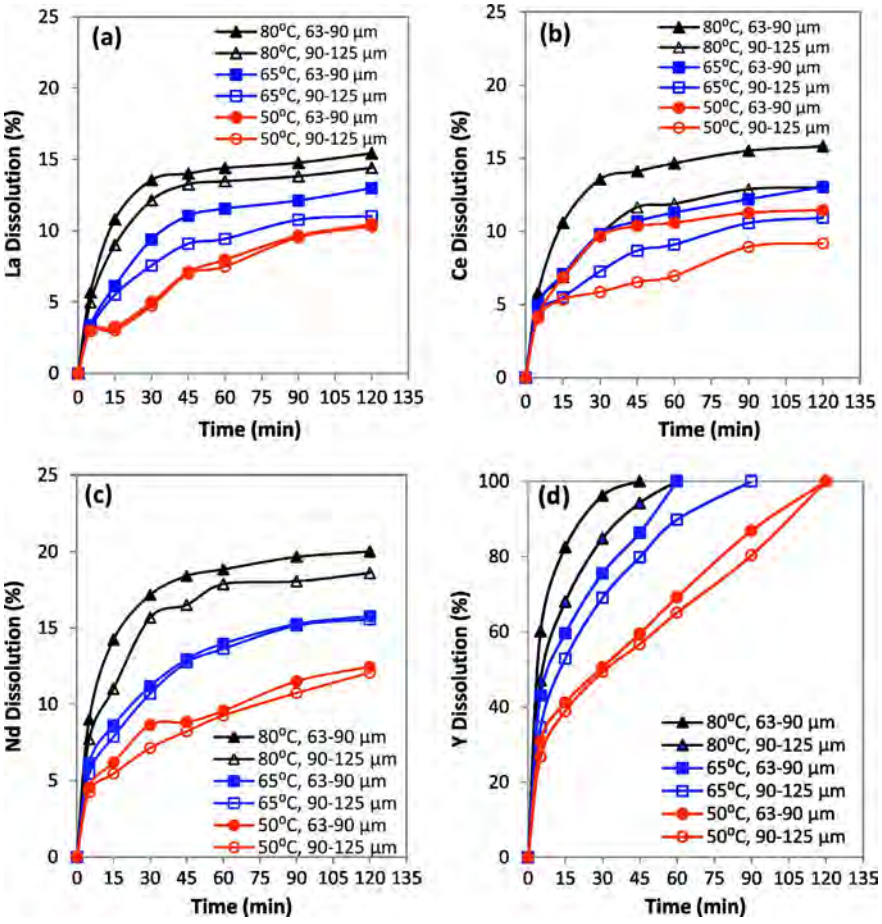

Fig. 2. Effect of leaching temperature and slag powder particle size on (a) La, (b) Ce, (c) Nd and (d) Y dissolution.

as well. In order to investigate the extraction yields of rare earth elements, a phase evaluation of both the initial material and the residues was performed with QEMSCAN (**Qu**antitative **E**valuation of **M**aterials by **SCAN**ning electron microscopy).

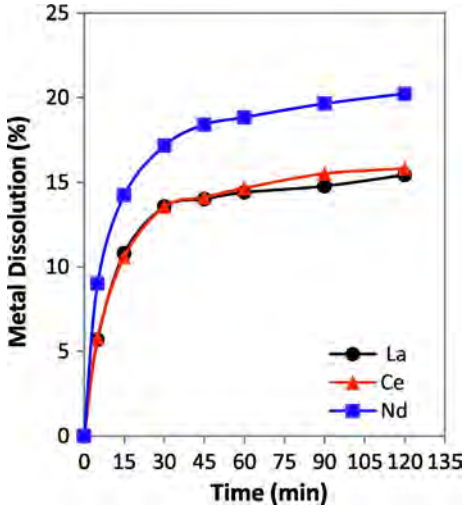

Fig. 3. Comparison of leaching efficiency of La, Ce and Nd for particle size 63–90 µm at 80 °C.

2. Experimental

2.1. Materials

The slag samples for this research study were prepared by the pyrometallurgical recycling process of NiMH batteries developed at The Institute of Process Metallurgy and Metal Recycling (IME) at RWTH Aachen University in Germany (Müller and Friedrich, 2006). Therefore, the IME top blown rotatory furnace (TBRC), with a capacity of one cubic meter, was used. After a preheating phase > 900 kg of NiMH batteries were charged with fayalite slag and some soda to lower the viscosity. As a reduction medium, to get a saleable metal phase, coke was added. After a total processing time of more than 7 h at about 1350 °C, a metal phase of about 150 kg and a slag phase of about 250 kg were tapped separately. The slag produced during the IME process for the recycling of NiMH batteries was used as the raw material for further experiments to extract the rare earth elements (REEs).

The ionic liquid, 1-methylimidazolium hydrogen sulfate ($HmimHSO_4$), whose chemical properties and structure are given in Appendix A was selected since the preliminary leaching test results showed that $HmimHSO_4$ is the most active ionic liquid among the other five acidic ionic liquids used for the leaching of the NiMH battery slag.

Table 2
Conversion-time expressions for spherical shapes of particles-shrinking core model.

(2) Diffusion through the liquid film	$\frac{t}{\tau} = X$
(3) Surface chemical reaction	$\frac{t}{\tau} = 1-(1-X)^{1/3}$
(4) Diffusion through the product layer	$\frac{t}{\tau} = 1-3(1-X)^{2/3}+2(1-X)$

(X: the reacted fraction, τ: time for complete reaction-min).

Table 3
Values of rate constants (slopes) and the correlation coefficients at different conditions.

Particle size (μm)	T (°C)	Fe		Mn	
		R^2	k (10^{-4} min^{-1})	R^2	k (10^{-4} min^{-1})
90–125	50	0.98	0.0008	0.96	0.0009
	65	0.99	0.0022	0.98	0.0031
	80	0.99	0.0060	0.98	0.0056
63–90	50	0.95	0.0039	0.96	0.0012
	65	0.97	0.0063	0.98	0.0029
	80	0.99	0.0099	0.99	0.0064

2.2. Leaching tests

The leaching experiments were carried out in closed beakers of 250 mL on a magnetic stirrer at specified temperatures. In each test, 25 g of slag powder was used with a volume of 250 mL aqueous 1-methylimidazolium hydrogen sulfate ionic liquid solutions which results in a constant pulp density of 10%. The $HmimHSO_4$ concentration of aqueous ionic liquid solution was 30% (v/v) in all tests. At selected time intervals, a solution sample of about 10 mL was taken out using a syringe filter. This slurry solution was filtered for solid liquid separation and the liquid part was analyzed by ICP-OES to determine the base and rare metal contents. The effects of dissolution temperature (50 °C, 65 °C and 80 °C) and particle size (63–90 μm and 90–125 μm) of the slag on the dissolution ratio of the elements were studied. Dissolution kinetics of base metals was also investigated.

2.3. QEMSCAN assisted assessment of leaching results

In order to explain the relatively low extraction yields of rare earth elements, a phase evaluation of the residues was performed with X-ray powder diffraction. As a result, no crystallographic phase could be identified which explains the low extraction yields. Experiments using the 1-methylimidazolium hydrogen sulfate ionic liquid solution to leach pure lanthanum oxide leads to an exothermic reaction and a lanthanum rich residue. The X-ray powder diffraction indicates an amorphous phase which explains the failed X-Ray powder diffraction analysis of the initial battery leach residues. To overcome this limitation of conventional X-ray powder diffraction analysis, QEMSCAN analysis (**Qu**antitative **E**valuation of **M**aterials by **SCAN**ning electron microscopy) of both the initial material and the leach residues was conducted at the Institute of Mineralogy and Economic Geology (RWTH Aachen University). This analytical method enables an X-ray based quantitative chemical mapping of the sample material and consists of a scanning electron microscope in combination with two energy-dispersive X-ray spectrometers. The field scan mode was applied for the data collection, which is an end to end chemical mapping of a defined area and resolution of the sample surface. Eighteen elements were chosen for measurement due to prior XRF and ICP-OES investigations. X-ray data was acquired every 5 μm (point spacing), collecting 2000-count EDX spectra on each analysis with an acceleration voltage of 25 keV and a specimen current of approximately 10 nA. Collected raw data was assigned to suitable phases by user-defined "must have" and "may have" elements with a specific concentration range for each phase using idiscover© software. During post processing, for every pixel, the software verifies if the conditions complied with the user definition, and allocates the pixels into the appropriate phases by a "true" or "false" validation. The accuracy of the phase boundaries was verified by overlapping BSE images. The QEMSCAN measurement results showed no difference between the coarse and fine fractions as related to occurring phases. In general, coarse material permits better results and produced less mixed spectra. Thus, the 90–125 μm fraction was used for further investigations. Two different samples ground slag and leach residue each with a grain size of 90–125 μm, were prepared onto thin sections.

3. Results and discussion

3.1. Characterization of NiMH batteries slag

A combination of operations was carried out for the slag using a jaw crusher and a ball mill, successively. Screening tests were performed on the ground slag powders in order to obtain two different particle size fractions: +63–90 μm and +90–125 μm. The samples from both the coarse and fine fractions were analyzed by Inductively Coupled Plasma Optical Emission Spectrometry (ICP-OES).

The chemical analysis of the slag powder with the particle size ranges of 63–90 μm and 90–125 μm is shown in Table 1.

The chemical analysis of the initial slag powders indicates that iron (35.70% w/w), aluminum (9.95% w/w) and manganese (3.45% w/w) are the major base metal elements. Other important elements are lanthanum, cerium, neodymium and yttrium (rare earth elements) in the ratio of about 10.00% w/w, 9.00%, 2.50% and 0.16%, respectively.

3.2. Leaching of base metals

The dissolution efficiency of iron at temperatures of 50 °C, 65 °C and 80 °C are shown in Fig. 1a. It is evident from Fig. 1a that the iron dissolution rate increased remarkably with increasing temperature from 50 °C to 65 °C. The particle size of the slag powders also has a significant effect on the iron leaching ratio as it increased from 50.3% to 70.7% with decreasing particle size range from 90–125 μm to 63–90 μm at 50 °C after 2 h. Similarly, iron dissolution increased from 70.7% to 90.8% upon decreasing the particle size range at 65 °C. Maximum Fe dissolution was attained at a temperature of 80 °C after 120 min for both particle sizes. Moreover, in the fraction with the particle size of 63–90 μm, almost all the iron was dissolved in the ionic liquid solution at 80 °C after 120 min. It is obvious that the iron leaching ratio increased with the decrease of particle size as the surface area per unit mass was increased.

The effect of temperature and particle size on the dissolution percentage of manganese over 2 h is shown in Fig. 2. The leaching temperature also has a significant effect on Mn dissolution and a maximum dissolution ratio (99.5%) reached at a higher temperature (80 °C). Mn dissolution rose from 57.7% to 65.2% with decreasing particle size from 90 to 125 μm to 63–90 μm at 50 °C. The effect of particle size was slight at 65 °C and 80 °C over 2 h. Leaching time and temperature dependence of Al dissolution from slag powder with particle size of 63–90 μm is shown in Fig. 1c, where it can be seen that Al dissolution is influenced marginally by increasing the temperature. Very similar behavior was also obtained from the slag powder with particle size of 90–125 μm (Fig. 1d). The decrease in dissolution of Al with the increase in leaching time for both particle size ranges indicated that aluminum precipitated with time during ionic liquid leaching.

3.3. Leaching of rare earth elements

The leaching of rare earth elements in 1-methylimidazolium hydrogen sulfate ionic liquid solutions was also investigated. The effect of temperature and particle size of slag powders on the leach efficiency of lanthanum is shown in Fig. 2a where it can be seen that the leaching of lanthanum is affected significantly by temperature and particle size of the battery slag powder under the conditions studied. At relatively low temperature (50 °C), dissolution of lanthanum was only about 10% for both ranges of particle sizes. This value increased with the increase in temperature and reached 13.0% and 15.4% at 65 °C and 80 °C, respectively for particle size of 63–90 μm. However, after 45 min the increase in dissolution ratio of La slowed down for all temperatures and both particle sizes.

The leaching efficiency results of cerium and neodymium are presented in Fig. 2b and c, respectively. The figures indicate that the

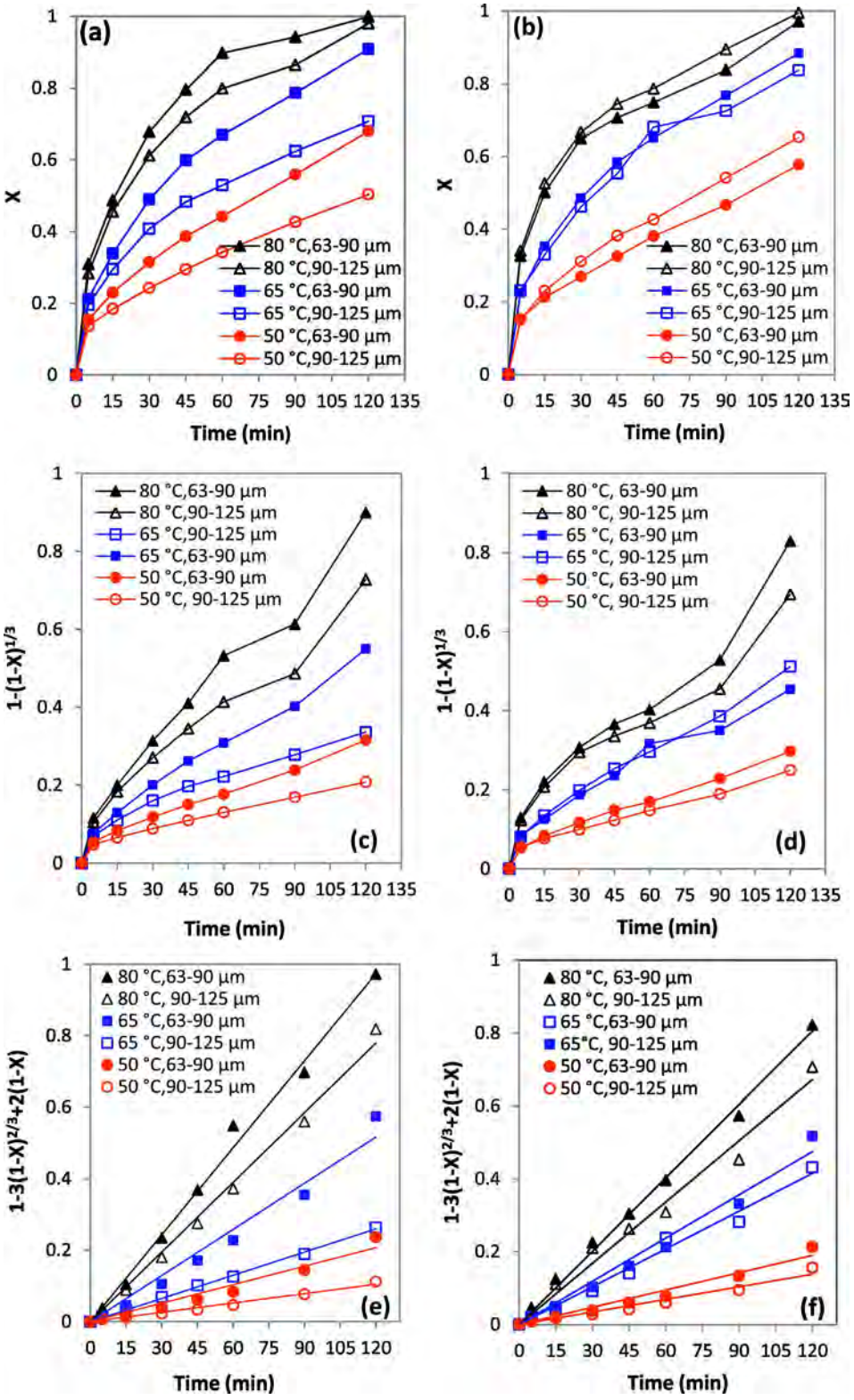

Fig. 4. Fitting of (a, c, e) Fe and (b, d, f) Mn dissolution (X) to several equations of the shrinking core model at various temperatures.

leaching efficiency of the metals increased sharply with the increase in leaching temperature. However, maximum cerium and neodymium leaching efficiencies were about 15% and 20%, respectively after 2 h in the operating range. The particle size of the slag powders also has an influence on the leaching behavior of both cerium and neodymium. Small particles (63–90 µm) indicated more efficient cerium and neodymium dissolution compared to large particles (90–125 µm) due to the increase in surface area per unit mass.

As shown in Fig. 2d, yttrium dissolution increased with decreasing particle size and increasing temperature. Yttrium leaching efficiency reached 100% for the 63–90 µm particle size at 80 °C after 45 min while dissolution was completed at the same temperature after

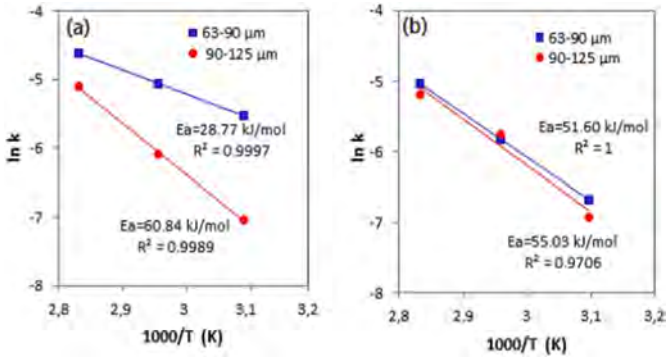

Fig. 5. Arrhenius plots for activation energy of a) Fe, b) Mn.

60 min for the 90–125 μm particle size. When the temperature was 50 °C, no significant difference was observed with increasing particle size. It means that recovery of yttrium from NiMH battery slag powder depends slightly on the particle size at low temperature.

Leaching behaviors of rare earth metals with particle size of 63–90 μm were compared in Fig. 3 at 80 °C. They all showed very similar trend during leaching test that their leaching efficiencies increased remarkably between 0 and 30 min and after that time increment slowed down considerably. In addition, La and Ce almost had same and low leaching efficiencies compared with Nd. The highest leaching efficiency was obtained with Nd in 120 min. as 20.2%.

3.4. Kinetic analysis

A leaching process is a heterogeneous reaction in which a liquid contacts and reacts with solid particles forming a product according to Eq. (1).

$$aA_{(fluid)} + bB_{(particle)} \rightarrow Product \quad (1)$$

Solid particles remain unchanged in size during reaction when they contain large amounts of impurities which remain as non-flaking ash or if they form a firm product material by the reaction of Eq. (1) (Quian et al., 2013). For such reaction systems, the reaction ratio is generally controlled by one of the following steps: (i) diffusion through the liquid film, (ii) diffusion through the ash/product layer and (iii) chemical reaction at the surface of the solid particles (Aydogan et al., 2006; Gharabaghi et al., 2012; Levenspiel, 1962; Safarzadeh et al., 2009). The slowest step of the reaction is quite well known as the rate-determining step.

In order to determine the kinetic parameters and rate controlling step for leaching of the slag powders in ionic liquid solutions, the experimental data was analyzed based on the shrinking core model using equations shown in Table 2 (Levenspiel, 1962).

The experimental data in Fig. 1a and b were examined based on Eqs. (2)–(4) shown in Table 3 and presented Fig. 4. As shown in Fig. 4e and f there is a linear correlation between the expression of $1-3(1-X)^{2/3}+2(1-X)$ and time for Fe and Mn dissolution and the rate control by diffusion of reagents or products through the product layer was found to fit the data better (Fig. 4e and f). The rate constants (slopes) and the correlation coefficients at different conditions were listed in Table 3.

The apparent rate constant k is a function of temperature and the relationship between k and T can be expressed by the Arrhenius equation (Kaplun et al., 2011).

$$k = k_0 \exp\left(\frac{-Ea}{RT}\right) \quad (5)$$

where k_0 is the frequency factor and Ea is the apparent activation energy. To calculate the activation energy, the Arrhenius plots of the leaching processes were plotted using the values of ln k against 1000/T.

According to the Arrhenius Eq. (5) and the slopes (−Ea/R) in Fig. 5, the apparent activation energies of the elements were calculated for small and large particles, respectively as about 28.8 kJ/mol and 60.8 kJ/mol for Fe; and 51.6 kJ/mol and 55.0 kJ/mol for Mn. In general the reactions controlled by diffusion should have low activation energy; therefore such values of activation energies are not typical for diffusion processes. High activation energy for the product layer diffusion controlled dissolution of minerals was also recognized rarely and it was appeared that its value may exceed 21.0 kJ/mol for the processes controlled by internal diffusion of reactants (Gbor et al., 2000; Baba et al., 2009; Paspaliaris and Tsolakis, 1987).

3.5. QEMSCAN assisted assessment of leaching results

The qualitative composition of identified phases is presented in Table 4. Four phases with a significant REE concentration were identified in the samples. They were divided into the different dominating elements Al, Fe and Si (Table 4). The sulfur dominated phase only occurs in the leach residue.

The other phases did not show a pertinent and consistent REE distribution and are dominated by Fe, Al, Mn and Cr, as can be observed in Table 4. Oxygen was principally detected. Major elements have to occur within all grains and at each measurement point of the defined phase, whereas minor elements may, or may not occur. All phases were characterized by a different composition and/or concentration of involved elements and therefore show a distinct brightness in the Back Scattered Electron (BSE) image, which was used as a validation parameter.

The distribution of grains in the ground slag is illustrated in Fig. 6a, b. Phases with a significant amount of REE show a higher BSE intensity because of their greater average atomic number. As can be seen in the false color and BSE image (Fig. 6a, b), the grain boundaries of identified phases are uniform.

The evaluation results of QEMSCAN raw data including identified phases and their quantitative distribution (in vol.%) in slag powder and leached slag powder are shown in Table 5.

The evaluation of the leaching experiments indicated a good leaching efficiency of iron and manganese with metal yields of >90%. In comparison, the extraction yields of the rare earth elements lanthanum, cerium and neodymium are under 20%. A comparison of the QEMSCAN analysis of the initial material (Fig. 6b) and the residue

Table 4
Identified phases and elemental composition.

Phase	Color	Major elements	Minor elements
Aluminum rich REE phase		Al, La, Ce, Nd, O	Fe, Si, Ca, K, Na, Co, Cr, Mn, Ni, Y, Zr
Iron rich REE phase		Fe, La, CeNd, O	Al, Si, Ca, K, Co, Cr, Mn, Ni, Y, Zr
Silicon rich REE phase		Si, Ca, La, Ce, Nd, O	Fe, K, Na, Co, Cr, Mn, Ni, Y, Zr
REE sulfate phase		S, Fe, La, Ce Nd, O	Al, Si, Ca, K, Na, Co, Cr, Mn, Ni, Y, Zr
Iron manganese phase		Fe, Mn, O	Al, Si, Ca, K, Na, Co, Ni, Y, Zr, La, Ce, Nd
Iron aluminum manganese phase		Fe, Al, Mn, O	Si, Ca, Na, Cr, Co, Mn, Ni, Y, Zr, La, Ce, Nd
Iron aluminum manganese chromium phase		Fe, Al, Mn, Cr, O	Ca, Na, Co, Ni, Y, Zr, La, Ce, Nd
Iron aluminum chromium nickel phase		Fe, Al, Cr, Ni, O	Si, Ca, Na, Mn, Co, Y, Zr, La, Ce, Nd
Silicon based transition phase		Si, Al, K, O	Fe, Ca, Mn, Ni, Co, Y, Zr, La, Ce, Nd
Aluminum phase		Al, O	Cr, Y

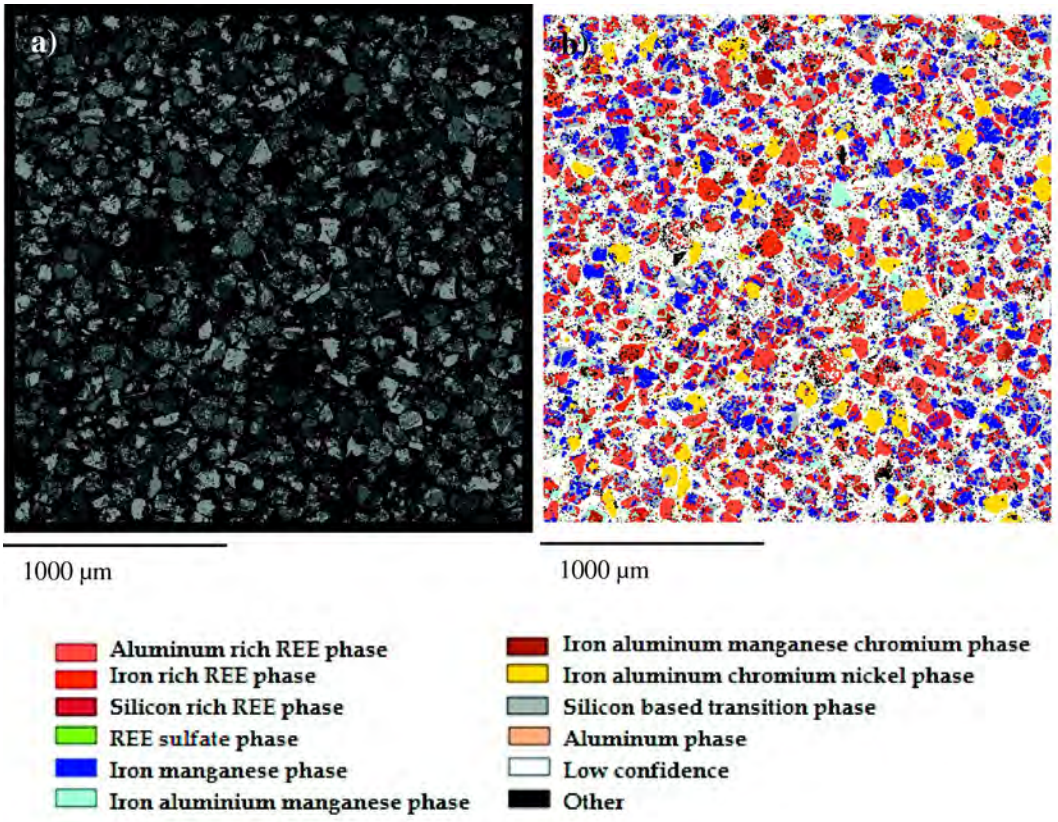

Fig. 6. a) BSE and b) false color image of ground slag. (For interpretation of the references to color in this figure legend, the reader is referred to the web version of this article.)

after leaching at 80 °C (Table 5 and Fig. 7b) indicates a material alteration of the phases. Due to the high recovery of iron and manganese, the iron manganese phase (blue), one of the dominant phases in the initial material (Fig. 6b), was almost dissolved (expected reaction 2) and barely present in the residue (Table 5 and Fig. 7b).

$$Mn_aO_b \cdot Fe_cO_d + 2(b+d)H^+ \rightleftarrows Mn^{x+}{}_{(aq)} + Fe^{y+}{}_{(aq)} + (b+d)H_2O \quad (2)$$

A similar behavior can be observed by the dominant rare earth phases. The iron rich REE phase (red) (expected reaction 3) and the silicon rich REE phase (wine-red) (expected reaction 4) were almost dissolved.

$$REE_2O_3 \cdot Fe_cO_d + 2(2+d)H^+ \rightleftarrows REE^{3+}{}_{(aq)} + Fe^{y+}{}_{(aq)} + (2+d)H_2O \quad (3)$$

$$REE_2O_3 \cdot SiO_2 + 6H^+ \rightleftarrows 2REE^{3+}{}_{(aq)} + Si(OH)_4 + H_2O \quad (4)$$

Only the aluminum rich REE phase (orange) was still present in the residue. In addition the evaluation of the QEMSCAN data with the compiled data base resulted in high rates of not matching phases, the low confidence phase (not shown in diagrams). Consequently a further phase with REEs has to be formed after leaching that might explain the low REE recovery rates.

Accordingly a further phase with sulfur, oxygen, the REEs and iron was implemented as "must have" elements. The result of the reanalysis indicated that this REE sulfate phase (green) is almost not present in the initial material but is the dominant phase in the residue (Table 4 and Fig. 6b). Therefore, a decomposition of the REE phases of battery slag powders by the ionic liquid 1-methylimidazolium hydrogen sulfate is possible. A direct precipitation as sulfates indicates by QEMSCAN is responsible for the low REE leaching efficiency. Moreover, the dissolution of REEs in acidic sulfate media is generally results low solubility due to the insoluble REE phases (Senanayake et al., 2016).

Table 5
Quantitative phase distribution within measured samples.

Phase	Phase volume (%)	
	Ground slag	Leach residue
Aluminum rich REE phase	12.18	11.36
Iron rich REE phase	19.11	1.81
Silicon rich REE phase	4.99	0.02
REE sulfate phase	2.83	57.94
Iron manganese phase	19.27	3.29
Iron aluminum manganese phase	8.17	10.11
Iron aluminum manganese chromium phase	2.96	4.31
Iron aluminum chromium nickel phase	6.84	7.41
Silicon based transition phase	13.76	0.01
Aluminum phase	0.03	0.01
Low confidence	3.50	1.83
Others	6.37	1.90

4. Conclusions

Rare earth elements lanthanum, cerium, neodymium and yttrium were found to exist in the structure of industrial NiMH spent battery recycling slag powders in additional to iron, manganese and aluminum. Ionic liquid $HmimHSO_4$ leaching provided high dissolution ratios for these base metals except Al. A decrease in the particle size of slag powder and an increase in temperature and time enhanced the dissolution ratios of La, Ce, Nd and Y. The shrinking core model with constant

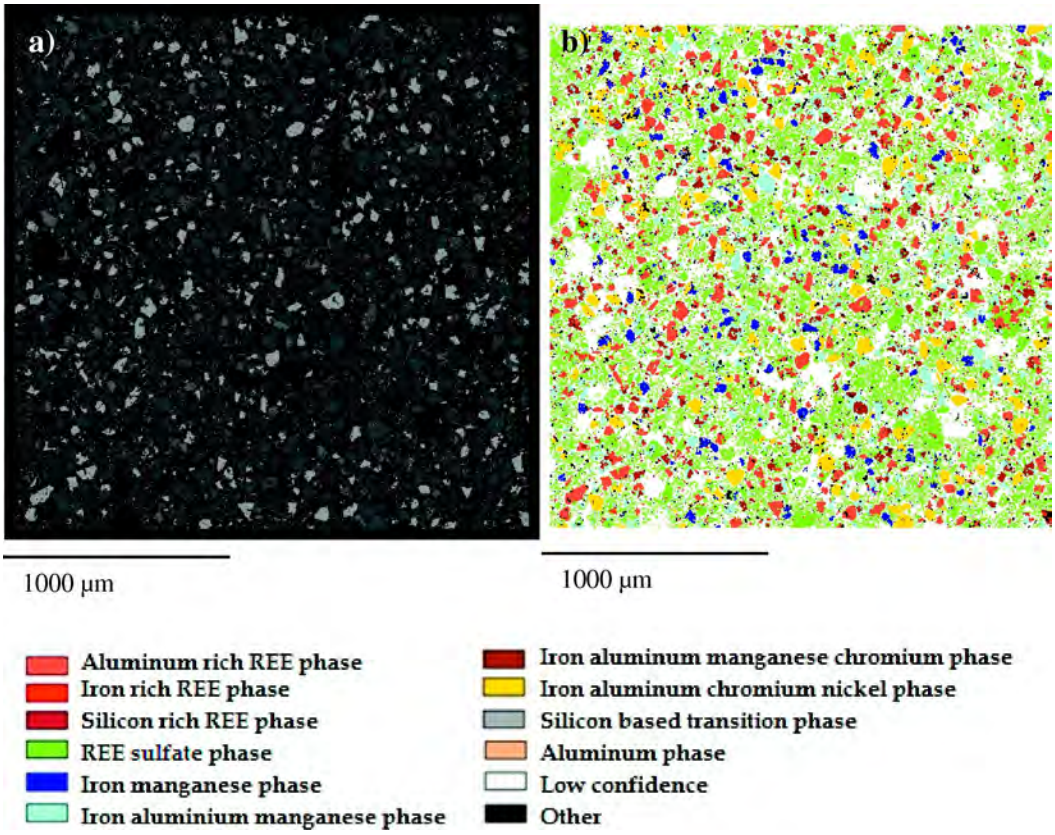

Fig. 7. a) BSE and b) false color image of leach residue after leaching at 80 °C. (For interpretation of the references to color in this figure legend, the reader is referred to the web version of this article.)

particle size found to be the best fit to the experimental data, and diffusion through the product layer seemed to be the rate controlling step for the leaching of Mn and Fe. The QEMSCAN analysis indicated that mineral decomposition of the REE phases of the battery slag by the ionic liquid $HmimHSO_4$ took place but direct precipitation as sulfates explains the low REE recovery rates.

Acknowledgments

We would like to thank The Scientific and Technological Research Council of Turkey (TUBITAK) for its research fellowship 2214A to support Ayfer Kilicarslan Sahin for a three-month stay at the IME Department of Process Metallurgy and Metal Recycling, RWTH Aachen University.

Appendix A

Table A1
Properties of ionic liquid $HmimSO_4$.

IL	$HmimHSO_4$
Name	1-Methylimidazolium hydrogen sulfate
Formula	$C_4H_6N_2 \cdot H_2SO_4$
Molecular weight	180.18 g/mol
Density at RT	1.4835 g/cm^3
Melting point	39 °C
Flash Point	>280 °C
Solubility in water	Soluble
Acidity/basicity	Acidic

Fig. 1A Structure of $HmimHSO_4$.

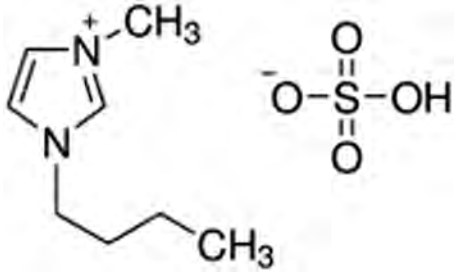

References

Al-Thyabat, S., Nakamura, T., Shibata, E., Lizuka, A., 2013. Adaptation of minerals processing operations for lithium-ion (LiBs) and nickel metal hydride (NiMH) batteries recycling: critical review. Miner. Eng. 45, 4–17.
Aydogan, S., Ucar, G., Canbazoglu, M., 2006. Dissolution kinetics of chalcopyrite in acidic potassium dichromate solution. Hydrometallurgy 81, 45–51.
Baba, A.A., Adekola, F.A., Toye, E.E., Bale, R.B., 2009. Dissolution kinetics and leaching of rutile ore in hydrochloric acid. JMMCE 10, 787–801.
Binnemans, K., Jones, P.T., Blanpain, B., Gerven, T.V., Yang, Y., Walton, A., Buchert, M., 2013. Recycling of rare earths: a critical review. J. Clean. Prod. 51, 1–22.
Dong, T., Hua, Y., Zhang, O., Zhou, D., 2009. Leaching of chalcopyrite with Brønsted acidic ionic liquid. Hydrometallurgy 99, 33–38.
Earle, M.J., Seddon, K.R., 2000. Ionic liquids. Green solvents for the future. Pure Appl. Chem. 72 (7), 1391–1398.
Gbor, P.K., Ahmed, I.B., Jia, C.Q., 2000. Behaviour of Co and Ni during aqueous sulphur dioxide leaching of nickel smelter slag. Hydrometallurgy 57, 13–22.
Gharabaghi, M., Irannajad, M., Azadmehr, A.R., 2012. Leaching behavior of cadmium from hazardous waste. Sep. Purif. Technol. 86, 9–18.
Guo-cai, T., Jian, L., Yi-xin, H., 2010. Application of ionic liquids in hydrometallurgy of nonferrous metals. Trans. Nonferrous Met. China 20, 513–520.
Han, D., Row, K.H., 2010. Recent applications of ionic liquids in separation technology. Molecules 15, 2405–2426.

Innocenzi, V., Vegliò, F., 2012. Recovery of rare earths and base metals from spent nickel-metal hydride batteries by sequential sulphuric acid leaching and selective precipitations. J. Power Sources 211, 184–191.
Itoh, M., Miura, K., Machida, K., 2009. Novel rare earth recovery process on Nd-Fe-B magnet scrap by selective chlorination using NH_4Cl. J. Alloys Compd. 477, 484–487.
Jordens, A., Cheng, Y.P., Waters, K.E., 2013. A review of the beneficiation of rare earth element bearing minerals. Miner. Eng. 41, 97–114.
Kaplun, K., Li, J., Kawashima, N.A., Gerson, R., 2011. Cu and Fe chalcopyrite leach activation energies and the effect of added Fe^{3+}. Geochim. Cosmochim. Acta 75, 5865–5878.
Kılıçarslan, A., Sarıdede, M.N., 2016. Leaching performance of imidazolium based ionic liquids in the presence of hydrogen peroxide for recovery of metals from brass waste. Rev. Metal. 52, e063.
Levenspiel, O., 1962. Chemical Reaction Engineering. second ed. Wiley, New York.
Massari, S., Ruberti, M., 2013. Rare earth elements as critical raw materials: focus on international markets and future strategies. Res. Policy 38, 36–43.
McCluskey, A., Lawrance, G.A., Leitch, S.K., Owen, M.P., Hamilton, I.C., 2002. Ionic liquids industrial applications for green chemistry. Am. Chem. Soc. 818, 199–212.
Müller, T., Friedrich, B., 2006. Development of a recycling process for nickel-metal hydride batteries. J. Power Sources 158, 1498–1509.
Paspaliaris, Y., Tsolakis, Y., 1987. Reaction kinetics for the leaching of iron oxides in diasporic bauxite from the Parnassus–Giona Zone Greece by hydrochloric acid. Hydrometallurgy 19, 259–266.
Pietrelli, L., Bellomo, B., Fontana, D., Montereali, M.R., 2002. Rare earths recovery from NiMH spent batteries. Hydrometallurgy 66, 135–139.
Quian, L., Zhang, B., Min, X.B., Shen, W.Q., 2013. Acid leaching kinetics of zinc plant purification residue. T. Nonferr. Metal Soc. 23, 2786–2791.
Safarzadeh, M.S., Moradkhani, D., Ojaghi-Ilkhchid, M., 2009. Kinetics of sulfuric acid leaching of cadmium from Cd-Ni zinc plant residues. J. Hazard. Mater. 163, 880–890.
Senanayake, G., Jayasekera, S., Bandara, A.M.T.S., Koenigsberger, E., Koenigsberger, L., Kyle, J., 2016. Rare earth metal ion solubility in sulphate-phosphate solutions of pH range −0.5 to 5.0 relevant to processing fluorapatite rich concentrates: effect of calcium, aluminium, iron and sodium ions and temperature up to 80 °C. Miner. Eng. 98, 169–176.
Welton, T., 1999. Room-temperature ionic liquids. Solvents for synthesis and catalysis. Chem. Rev. 99, 2071–2084.
Weyhe, R., Friedrich, B., Heegn, H.P., Müller, T., 2002. Feasibility of a new closed loop recycling concept for Nickel-Metalhydride Batteries. Int. Battery Recycling Cong, Vienna, Austria, pp. 1–26.
Whitehead, J.A., Lawrence, G.A., McCluskey, A., 2004. Green leaching: recyclable and selective leaching of gold-bearing ore in an ionic liquid. J. Green Chem. 6, 313–315.
Whitehead, J.A., Zhang, J., Pereira, N., McCluskey, A., Lawrance, G.A., 2007. Application of 1-alkyl-3-methyl-imidazolium ionic liquids in the oxidative leaching of sulphidic copper, gold and silver ores. Hydrometallurgy 88, 109–120.
Xie, F., Zhang, T.A., Dreisinger, D., Doyle, F., 2014. A critical review on solvent extraction of rare earths from aqueous solutions. Miner. Eng. 56, 10–28.